UC Riverside
2017 Publications

Title
Modeling the Dispersion of Pollutants in Vicinity of Depressed Roadways

Permalink
https://escholarship.org/uc/item/1026t6d7

Authors
Amini, Seyedmorteza
Venkatram, Akula
Heist, David
et al.

Publication Date
2017-06-01

Peer reviewed

Modeling the Dispersion of Pollutants in Vicinity of Depressed Roadways

Conference Paper · June 2017

4 authors, including:

Seyedmorteza Amini
University of California, Riverside
5 PUBLICATIONS **2** CITATIONS

SEE PROFILE

Akula Venkatram
University of California, Riverside
173 PUBLICATIONS **3,166** CITATIONS

SEE PROFILE

Some of the authors of this publication are also working on these related projects:

Dispersion of Roadway emissions View project

Effectiveness of Sound Wall-Vegetation Combination Barriers as Near-Roadway Pollutant Mitigation Strategies View project

Modeling the Dispersion of Pollutants in Vicinity of Depressed Roadways

Seyedmorteza Amini, Akula Venkatram
Department of Mechanical Engineering, University of California, Riverside, CA, USA
David K. Heist, Steven G. Perry
US EPA, Office of Research and Development, National Exposure Research Laboratory, Research Triangle Park, NC, USA

ABSTRACT

This paper presents an analysis of wind tunnel experiments on depressed roadways and the development of a semi-empirical Gaussian dispersion model that captures the essential effects of depressed roadways on the flow field and dispersion of roadway-emitted pollutants. Four different configurations of depressed roadways are studied: a 6 m deep depressed roadway with vertical sidewalls (case 1), a 6 m deep depressed roadway with 30° sloping sidewalls (case 2), a 9 m deep depressed roadway with vertical sidewalls (case 3), and a 6 m deep depressed roadway with 30° sloping sidewalls with presence of two 6 m solid barriers on top of the road (case 4). All configurations change the flow field and decrease concentrations downwind of the road compared to the flat terrain case; however, the degree to which each case alters the flow field and decreases concentrations depends on how complex the configuration is. For example, the highest concentration reduction is observed in case 4.

A model is developed to estimate the surface concentrations downwind of the road for the aforementioned cases. The Depressed Road Model is based on the following principles: 1) the depressed roadway increases initial mixing height, 2) assuming the same depth for two roads, the initial mixing height is larger for the road with steeper sidewalls, 3) adding barriers increases the initial mixing height, and 4) the depressed road increases the rate of increase of dilution. However, initial mixing height does not increase linearly with the road depression. This model performs well in predicting surface concentrations downwind of the depressed roads. The model also predicts the surface concentration ratios of different cases reasonably well.

Keywords: Near-road air quality, Dispersion modeling, Depressed roadway, Line Source, Wind Tunnel Experiment.

INTRODUCTION

Recent studies have reported that living in vicinity of roadways results in adverse health effects[1]. Roadways can be elevated, depressed, or at-grade with surroundings. Different types of

obstacles, such as noise barriers and/or vegetative barriers, might be present next to the roadways as well. Several studies have examined the effects of presence of solid and vegetative barriers next to freeways on mitigating traffic-related pollutants[2–10]. The effects of freeway depression on dispersion of traffic-related pollutants, though critical, have been barely studied. Modeling concentration data in vicinity of a depressed roadway enables us to facilitate the analysis of real-world concentration data collected in complex urban environments.

In one of the few studies on depressed roadways, particulate lead concentrations in vicinity of a flat terrain and a depressed roadbed configuration were measured[11]. The samplers were placed upwind of the freeway and at locations downwind of the freeway up to 160 m from the median strip. It was observed that the mass concentrations of traffic-derived aerosols were lower downwind of depressed roadbed configurations than the theoretical dispersion model predictions for at-grade configurations.

To investigate the effects of a depressed roadway on local-scale air quality, a field study was conducted in Las Vegas, NV[12]. CO and NO_2 concentrations along a complex urban highway were measured at two sections; a section at-grade with the surroundings and another section with depressed configuration. The vertical height from the roadbed to the top of the surroundings was 5 m, and the angle between sidewalls and the road was 70°. The collected data along the highway indicated that the peak concentrations occurred with the flat terrain configuration, while average simultaneous concentrations are higher in the depressed roadway configuration, which occurred mostly during lower pollutant events. The researchers also conducted a wind tunnel simulation of the study site. They observed that the cut section reduced concentrations of pollutants by 15 – 25% for receptors located approximately 20 m from the highway. The concentrations continued to be lower for the depressed roadway relative to the at-grade roadway over the entire downwind domain. Venkatram et al. analyzed the Las Vegas data using dispersion models[13]. They used an analytical approximation to estimate the concentrations due to the line source[14] with one modification; they accounted for the increase in vertical mixing of the plume by assuming that the initial mixing height of the plume is equal to the depression of the road, 5 m. However, they stated that this empirical adjustment has to be evaluated with other experimental results.

Industrial Source Complex (ISC3) Dispersion Models describe a model that is able to predict concentrations downwind of a below-grade open pit, such as a surface coal mine[15]. The main assumption in this model is that the recirculation zone within the pit causes the particles to emit from the leeward side of the pit, resulting in an upwind source shift. While the aspect ratio (length/width) of a depressed roadway is infinity, this model is only valid for the open pits with the aspects ratios of up to 10 to 1.

In this study, we present results from a wind-tunnel study[16] and observations on the effects of different road configurations, including depressed roadways, on flow field and dispersion of roadway-emitted pollutants. Then we develop a semi-empirical Gaussian dispersion model that is able to predict the surface concentrations downwind of different configurations of depressed roadways reasonably well. We then examine the model performance in predicting the ratios of surface concentrations of different cases.

EXPERIMENTAL METHODS

A wind tunnel study was performed in the U.S. EPA's Fluid Modeling Facility meteorological wind tunnel to explore the effects of different road configurations on the dispersion of traffic-related pollutants downwind of the roads[16]. This study examined twelve roadway configurations. The line source is a six lane divided highway at a 1:150 scale. The origin of the coordinate system is at the center of the roadway on wind tunnel floor, with positive x is the streamwise direction, y along the axis of the roadway, and z vertically upward.

The configurations that are studied in this paper are shown in Figure 1. We examine a 6 m deep depressed roadway with vertical sidewalls (case 1), a 6 m deep depressed roadway with 30° sloping sidewalls (case 2), a 9 m deep depressed roadway with vertical sidewalls (case 3), and a 6 m deep depressed roadway with 30° sloping sidewalls with presence of two 6 m solid barriers on both sides of the road (case 4) as four different depressed road configurations. We also compare the effects of these configurations with observations in flat terrain case (case 0), a 6 m solid barrier downwind of a flat road case (case 5), and 6 m double solid barriers on the sides of a flat road case (case 6).

Figure 1- Elevation view showing cross sections through the different roadway designs studied; a) flat terrain roadway (case 0), b) 6 m deep depressed roadway with vertical sidewalls (case 1), c) 6 m deep depressed roadway with 30° sloping sidewalls (case 2), d) 9 m deep depressed roadway with vertical sidewalls (case 3), e) 6 m deep depressed roadway with 30° sloping sidewalls with added double noise barriers (case 4), f) 6 m downwind noise barrier (case 5), and g) 6m double noise barriers (case 6).

g)
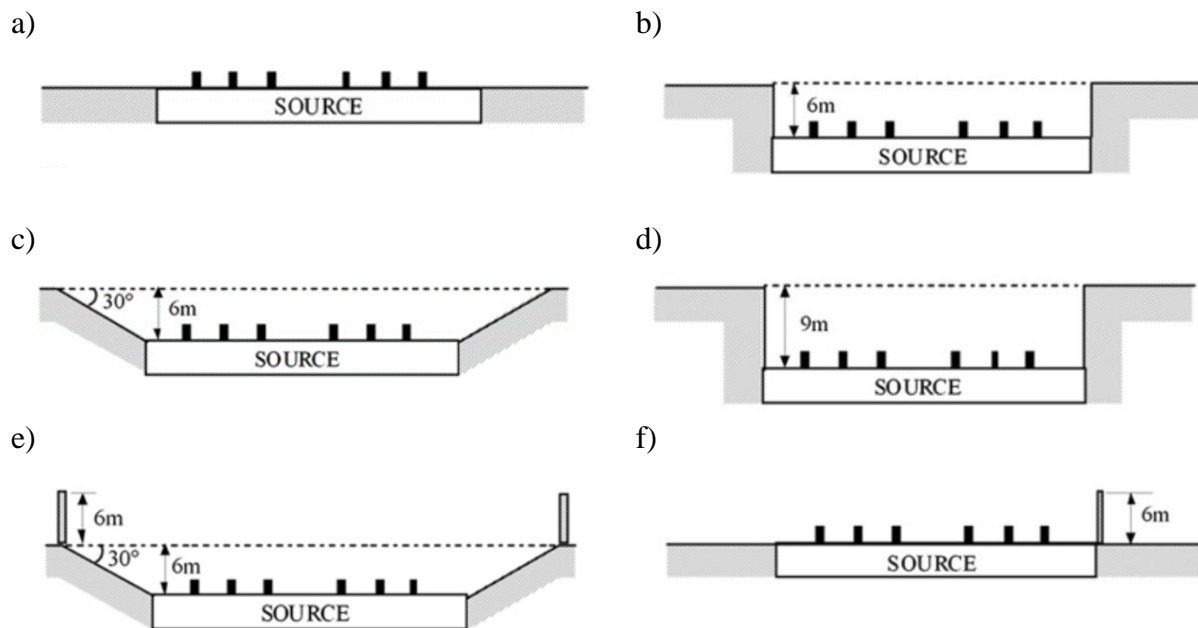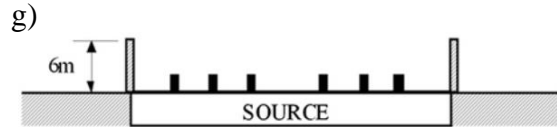
The tracer gas used in the study was high-purity ethane (C_2H_6). The concentrations of ethane were normalized to give the non-dimensional concentration $\chi = CU_r/(Q/L_xL_y)$, where C is the concentration (a fraction by volume) with background concentration subtracted, U_r is the reference wind speed (equal to 2.46 m/s, measured at a full-scale equivalent height of 30 m), Q is the volumetric effluent rate (1500 cm^3/min of ethane), L_x is the alongwind dimension of the roadway segment (24 cm, 36 m full scale), and L_y is the lateral length of the source segment (48 cm, 72 m full scale).

EXPERIMENTAL RESULTS

Heist et al. presented the impacts of different road configurations on the flow field and the concentration field[16]. Here, we focus on the depressed road configurations.

1.   Impact of road depression on the flow field

Flow field was affected by the road configurations. The impact of road configurations on the flow field is shown in Figure 2. The depressed roadway with 30° sloping sides (case 2) has the least effect on the flow field, causing no mean recirculation in the depressed region. The depressed roadways with vertical sidewalls (cases 1 and case 3) create recirculating flow in the depressed regions, with a stronger recirculation in the deeper road cut case (case 3). The depressed roadway with 30° sloping sides and double noise barriers (case 4) create the strongest recirculating flow amongst all cases. Cases with stronger recirculation region cause more intense upward deflection of particles.

Figure 2- Observed mean velocity vectors for a) case 1, b) case 2, c) case 3, d) case 4.

a)

b)

c)

d)
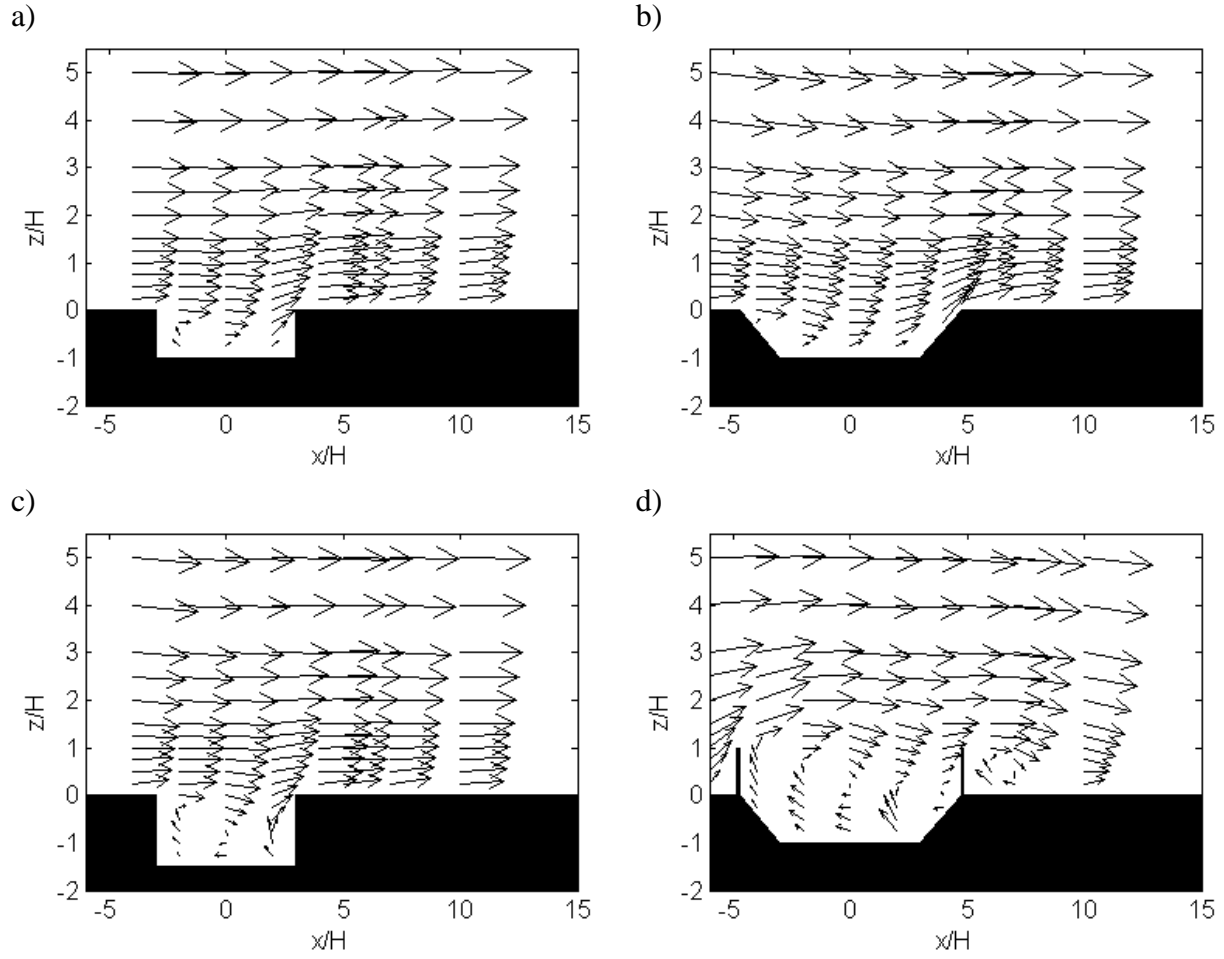
Figure 3- Surface concentration gradients for different configurations. Left plot includes flat terrain concentrations.

a)

b)
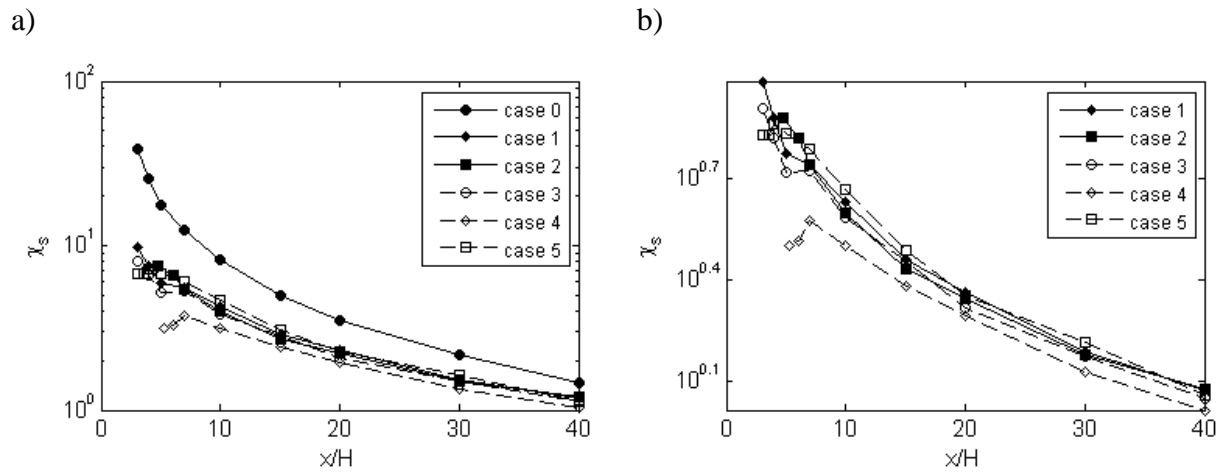
As mentioned before, two of the configurations studied in the wind tunnel study investigate the effects of a single downwind noise barrier and double noise barriers next to a road on the flow field and the concentrations downwind of the road. Here, we compare the effects of road depression with the effects of a single barrier and double barriers next to roads. The ratio of the surface concentrations downwind of the roadway with barriers (single or double) to the depressed roadway is shown in Figure 4. Surface concentrations downwind of a flat road with a single downwind barrier (case 5) is around 5% lower than those downwind of a depressed road (case 1) very close to the road (at $x = 4H$). The surface concentration ratios of case 5 to case 1 become larger between $x = 5H$ and $x = 15H$ with the maximum value of 115%, and converge to unity after $x = 15H$. Surface concentrations downwind of double noise barriers (case 6), compared to case 1, are 20% lower very close to the road ($x = 4H$). The surface concentration ratios of case 6 to case 1 follow a sudden increase which results in the value of 97% at $x = 5H$ and become larger than unity after $x = 10H$. The differences between case 5 and case 1, and case 6 and case 1 are lower than 10% at the end of the domain, where the effects of road configurations fade away.

Figure 4- Ratio of surface concentrations. Solid line represents ratio of surface concentrations of case 5 to case 1, whereas dashed line represents that of case 6 to case 1.
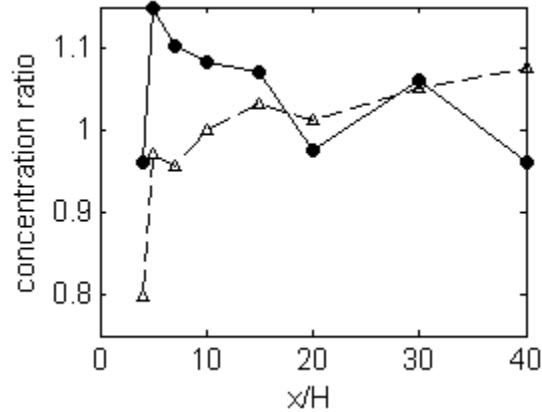
DEPRESSED ROAD MODEL

1.   Framework for the model

A Gaussian plume model was used to analyze the surface concentration data. The Gaussian plume formulation for a point source gives the concentration as:

$$C(x,y,z) = \frac{Q}{\sqrt{2\pi}\sigma_y(x)} \exp\left(-\frac{y^2}{2\sigma_y(x)^2}\right) F_z(x,z) \tag{1}$$

where x is the downwind distance from the point source, y is the crosswind distance from the source, z is the height of the receptor, Q is the emission rate, σ_y is the horizontal plume spread at downwind distance x, and F_z is the vertical distribution function, defined as:

6

$$F_z(x,z) = \frac{1}{U(\bar{z})\sqrt{2\pi}\sigma_z(x)}\left[\exp\left(-\frac{(z-h)^2}{2\sigma_z(x)^2}\right) + \exp\left(-\frac{(z+h)^2}{2\sigma_z(x)^2}\right)\right] \qquad (2)$$

where σ_z is the vertical plume spread at the downwind distance x, h is the source height, and $U(\bar{z})$ is the wind speed evaluated at the mean plume height, $\bar{z}$, defined as:

$$\bar{z} = \frac{\int_0^\infty zC^y(x,z)dz}{\int_0^\infty C^y(x,z)dz} \qquad (3)$$

where $C^y(x,z)$ is the crosswind integrated concentration. Mean plume height for a Gaussian plume can be calculated as[17]:

$$\bar{z} = \sigma_z\sqrt{\frac{2}{\pi}}\exp\left[-\frac{1}{2}\left(\frac{h}{\sigma_z}\right)^2\right] + h\,\mathrm{erf}\left(\frac{h}{\sqrt{2}\sigma_z}\right) \qquad (4)$$

Line sources are treated as sets of point sources. Therefore, the concentration in proximity of a line source is calculated by integrating Equation 1. This integral can be evaluated analytically when wind blows perpendicular to the line source ($\theta = 0°$), as air does in the wind tunnel, and it gives concentration as:

$$C(x,y,z) = \frac{q}{2}.F_z(x,z)[\mathrm{erf}(t_1) - \mathrm{erf}(t_2)] \qquad (5)$$

where q is the line source emission rate per unit length, x is the perpendicular distance of the receptor from the source, and t_1 and t_2 under perpendicular wind direction are defined as:

$$t_i = \frac{(y - y_i)}{\sqrt{2}\sigma_y} \qquad (6)$$

where the subscripts refer to the two ends on the line source, and $y - y_i$ is the distance of the receptor from the two ends of the source. For an infinitely long line source, values of t_1 and t_2 are ∞ and $-\infty$, respectively, which simplifies Equation 5 to:

$$C(x,z) = q.F_z(x,z) \qquad (7)$$

Now, the vertical plume spread used in $F_z(x,z)$ formulation is calculated by:

$$\sigma_z = \sqrt{h_0^2 + \sigma_{zF}} \qquad (8)$$

where h_0 is the initial mixing height, and σ_{zF} is the vertical plume spread calculated using plume spread formulations[17]. σ_{zF} for the neutral conditions is:

$$\sigma_{z_F} = 0.57\alpha \frac{u_*}{U(\bar{z})} x \tag{9}$$

where u_* is the surface friction velocity. We include the factor α to account for the larger rate of increase of dilution over distance in complex environments.

The Depressed Road Model (DRM) is based on the following principles: 1) the depressed roadway increases initial mixing height proportional to the depth of the road, 2) assuming the same depth for two roads, the initial mixing height is larger for the road with steeper sidewalls, 3) adding barriers increases the initial mixing height, and 4) the depressed road increases the rate of increase of dilution. We discuss how to incorporate these principles into the model in the next section.

2. Interpretation of the concentration data within the model framework

One way to find the initial mixing height and α, is to plot dilution, $U\sigma_z$, against downwind distance for different cases. The dilution is related to the entrainment velocity (w_e)[16] by $w_e = d(U\sigma_z)/dx$ [5]. Since the source height is zero, dilution for each case and at each distance from the source can be calculated by knowing the maximum concentration at that distance:

$$U\sigma_z = \sqrt{\frac{2}{\pi}} \frac{q}{C_m(x)} \tag{10}$$

where $C_m(x)$ is the maximum concentration at each downwind distance. Figure 5 shows the plot of dilution against the distance from the source. The initial vertical plume spread is indicated by the y-intercept of the plots. Figure 5 shows that the initial vertical plume spreads of complex cases are larger than that of flat terrain. The degree to which each case increases initial plume spread depends on how different the case is from the flat terrain case. Based on Equation 8 and Equation 9, the effect of initial mixing height on concentrations decreases over downwind distance. Using the concentration data, we find the value of h_0 for each case (
Table 1). This table satisfies the principles 1-3 that were pointed out in the previous section.

Figure 5- Dilution against distance from the source for different cases in wind tunnel study.
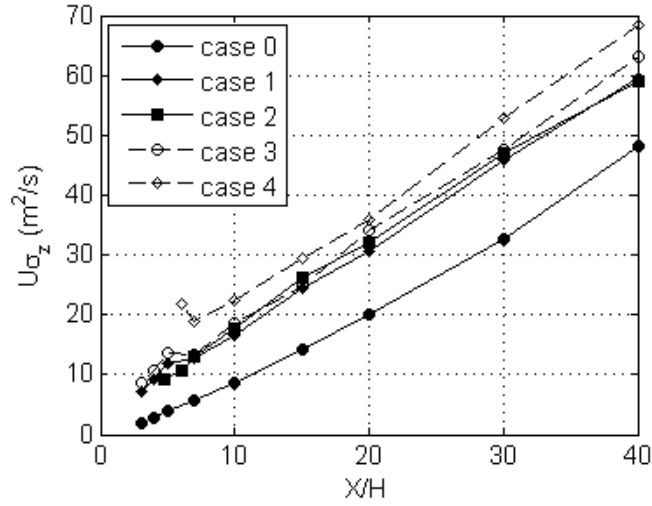
Table 1- Value of initial mixing height for different depressed road cases.

Case #	$h_0(m)$
1	7
2	6
3	8.5
4	11.5

Based on Equation 8 and $w_e = d(U\sigma_z)/dx$, the ratio of the entrainment velocities of one case to that of the flat terrain converges to α at far distances and is larger than α at small distances. A plot of these ratios for different cases is shown in Figure 6. We formulate α as an exponential function with the initial value of 2 and final value of 1, in the following form:

$$\alpha = \alpha_0 + (1 - \alpha_0)\left(1 - \exp\left(-\frac{x}{L_s}\right)\right) \tag{11}$$

where $\alpha_0 = 2$, and $L_s = 30h_0$.

Figure 6- The ratio of entrainment velocity of various cases to the entrainment velocity of the flat terrain at multiple downwind locations.
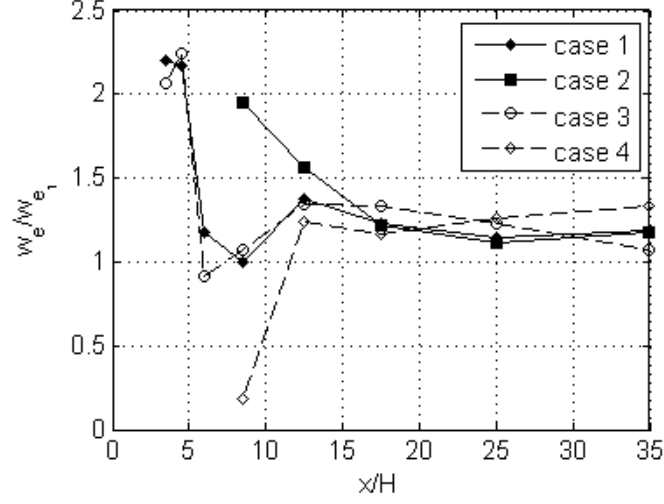
RESULTS AND DISCUSSION

The performance of the model is evaluated using the geometric mean (m_g), standard deviation of the residuals between the observations and predictions (s_g), the fraction of data points within a factor of two of the observations (*fact2*), and the correlation coefficient between the observations and predictions (r^2)[18]. The geometric mean and standard deviation are defined as:

$$\ln m_g = \sum_i \frac{\epsilon_i}{N} \tag{12}$$

$$\ln s_g = \sqrt{\frac{\sum_i (\epsilon_i - \ln m_g)^2}{N-1}} \tag{13}$$

where $\epsilon_i = \ln(C_{obs.}) - \ln(C_{pred.})$ is the residual between the observed concentration data and the predicted one, and N is the number of data points.

The performance of the model in predicting the ground-level concentrations of different cases is indicated in the scatterplots in Figure 7. The scatterplots show that the model is able to predict the surface concentrations of different cases properly. The model is unbiased for all cases ($m_g \simeq 1$) and the deviations of the model estimates from the observations are very small ($s_g \simeq 1$). All the predicted concentrations lie within a factor of two limit of the observed values, and the model correlates with the observations very well ($r^2 \simeq 1$).

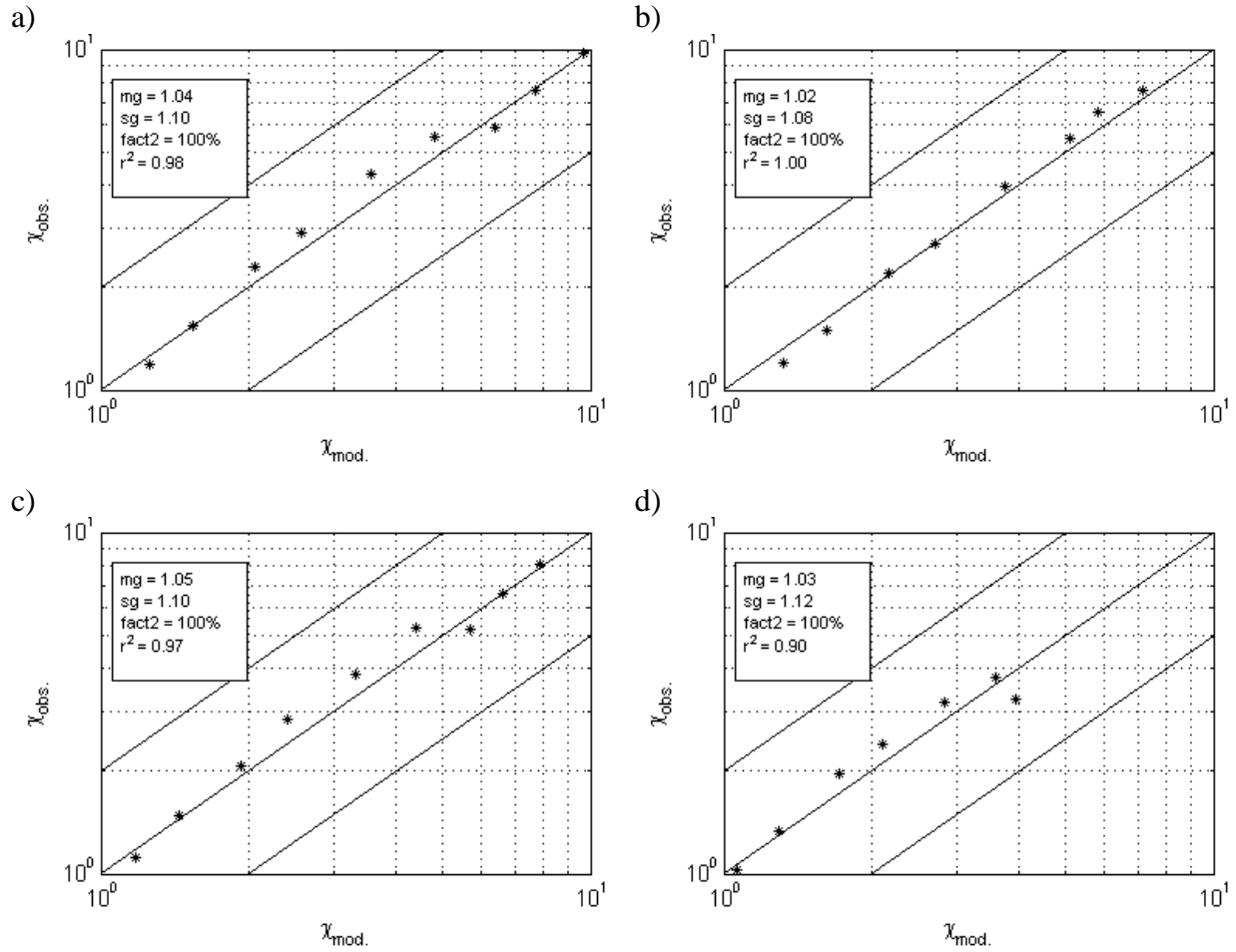**Figure 7- Comparison of the model estimates and observations in a) case 1, b) case 2, c) case 3, and d) case 4.**

a)

b)

c)

d)

Figure 8, which compares the observed ground-level concentration gradients with model estimates in different cases, indicates that the model performance in predicting the concentration gradient for different configurations, which includes various road depths and sidewall angles, is acceptable.

Figure 8- Comparison of observed and estimated concentration gradients in a) case 1, b) case 2, c) case 3, and d) case 4.

a)   b)
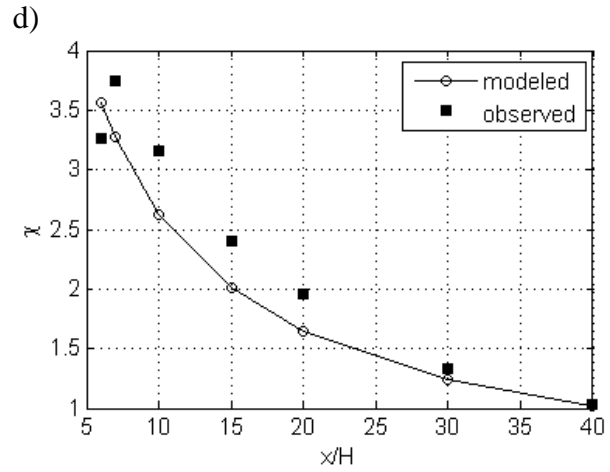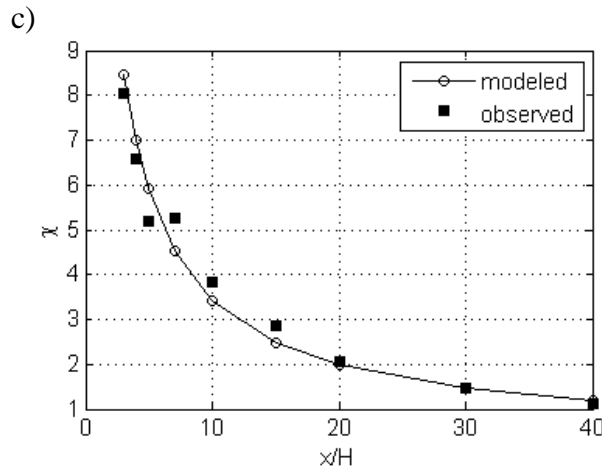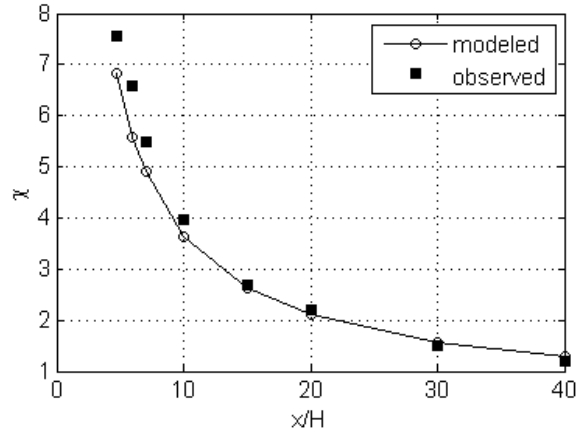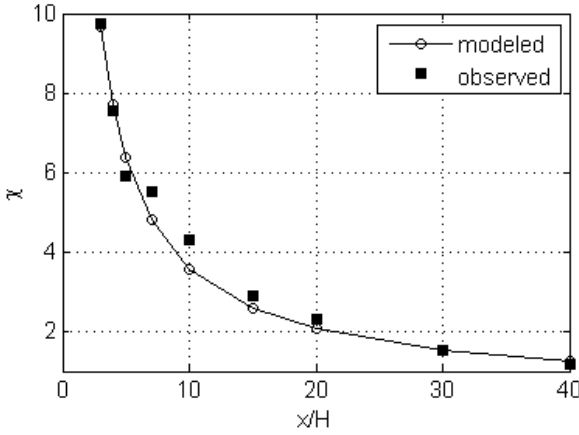
The model performance is acceptable if it is able to predict the correct surface concentration ratios of different cases. For example, if observations show that increasing road depression from 6 m to 9 m causes surface concentration at $x = 10H$ to decrease by 11%, the model should indicate this as well. We consider case 1 as the control case and compute the observed and modeled ratios of surface concentrations of cases 2, 3, and 4 to the control case. Figure 9 shows the plots of these ratios over downwind distance. Surface concentrations of case 2 are larger than the surface concentrations of case 1 immediately downwind of the road, become smaller, and eventually converge to the surface concentrations of case 1. Depending on the value of h_0 for each case, the model can either predict ratios below 1 or above 1 for the entire domain. Since h_0 value of case 2 is lower than that of case 1, the ratio of surface concentrations of case 2 to case 1 remains above 1. In case 3, all surface concentrations are lower than the corresponding surface concentrations of the control case. As expected, the largest difference occurs very close to the road with around 20% reduction. The concentration ratio converges to 1 at further distances. As Figure 9b indicates, the model is capable of predicting the concentration ratios of case 3 to the control case. In case 4, the surface concentrations are lower than those of the control case over the entire domain. The observed ratio is lower than the modeled ratio close to the road because the model overpredicts surface concentrations of case 4 at the receptors very close to the road. Overall, the model is able to capture the effect of depression and adding noise barriers on top of the road.

Figure 9- Ratio of surface concentrations of a) case 2, b) case 3, and c) case 4 to those of case 1 over downwind distance. Solid lines represent measured values and dashed lines are the modeled values.

a)

b)

c)
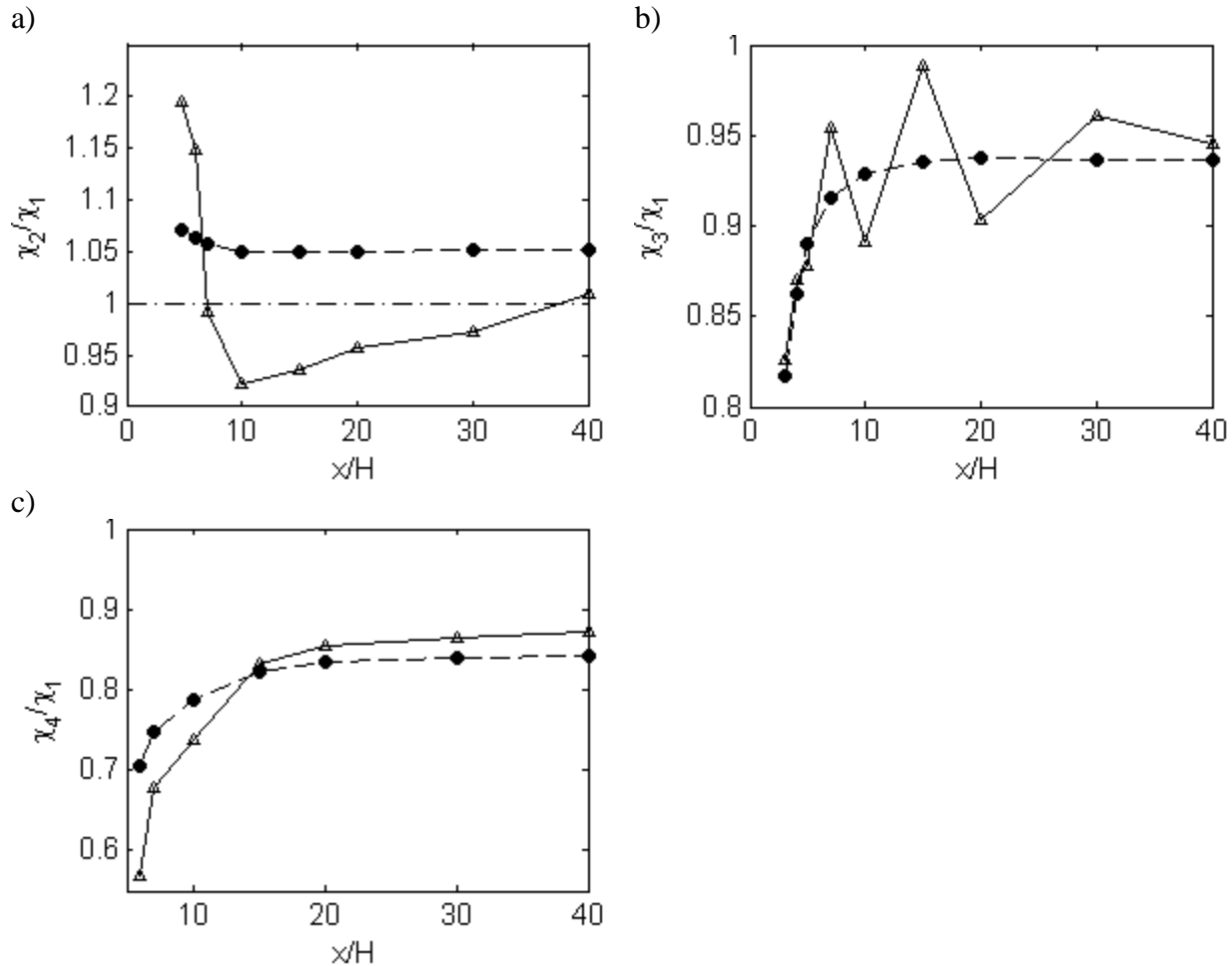
SUMMARY

We used data from a wind-tunnel study to develop a dispersion model, Depressed Road Model (DRM), that parameterizes the effects of depressed roadways on dispersion. Twelve different configurations were studied in the wind tunnel measurements, in which four cases examined the effects of depressed roadways on dispersion. The DRM accounts for the essential effects of the depressed roadways on pollutant dispersion. The model is based on the following principles: 1) the depressed roadway increases initial mixing height proportional to the depth of the road, 2) assuming the same depth for two roads, the initial mixing height is larger for the road with steeper sidewalls, 3) adding barriers increases the initial mixing height, and 4) the depressed road increases the rate of increase of dilution.

The DRM is able to estimate the ground-level concentrations downwind of multiple configurations of depressed roads. Since the model is based on the wind-tunnel results, it has been evaluated to work under neutral conditions and winds perpendicular to the road. The model also predicts the surface concentration ratios of different cases reasonably well.

The important factor that determines the efficacy of depressed roadways in mitigating air pollution near roadways is the initial mixing height. We found the initial mixing height of each case by using the concentration data. The initial mixing height is not linearly proportional to the road depression; increasing depression from 6 m to 9 m causes an increase in h_0 by 1.5 m. To model any depressed road case, we need to formulate h_0 as a function of the road depression, the angle between sidewalls and the roadbed, and the height of the solid barrier. To do so, more data on different configurations are needed.

REFERENCES

(1) HEI. Boston, MA 2010.
(2) Heist, D. K.; Perry, S. G.; Brixey, L. A.; Thompson, R. S.; Bowker, G. E. *Wind Tunnel Simulation of Flow and Dispersion near Urban Roadways*; 2007.
(3) Finn, D.; Clawson, K. L.; Carter, R. G.; Rich, J. D.; Eckman, R. M.; Perry, S. G.; Isakov, V.; Heist, D. K. *Atmos. Environ.* **2010**, *44* (2), 204–214.
(4) Amini, S.; Ahangar, F. E.; Schulte, N.; Venkatram, A. *Atmos. Environ.* **2016**, *138*, 55–64.
(5) Schulte, N.; Snyder, M.; Isakov, V.; Heist, D.; Venkatram, A. *Atmos. Environ.* **2014**, *97*, 286–295.
(6) Hagler, G. S. W.; Lin, M. Y.; Khlystov, A.; Baldauf, R. W.; Isakov, V.; Faircloth, J.; Jackson, L. E. *Sci. Total Environ.* **2012**, *419*, 7–15.
(7) Steffens, J. T.; Heist, D. K.; Perry, S. G.; Isakov, V.; Baldauf, R. W.; Zhang, K. M. *Atmos. Environ.* **2014**, *94*, 74–85.
(8) Steffens, J. T.; Heist, D. K.; Perry, S. G.; Zhang, K. M. *Atmos. Environ.* **2013**, *69*, 76–85.
(9) Steffens, J. T.; Wang, Y. J.; Zhang, K. M. *Atmos. Environ.* **2012**, *50*, 120–128.
(10) Ahangar, F. E.; Heist, D.; Perry, S.; Venkatram, A. *Atmos. Environ.* **2017**, *155*, 1–10.
(11) Feeney, P. J.; Cahill, T. A.; Flocchini, R. G.; Eldred, R. A.; Shadoan, D. J.; Dunn, T. *J. Air Pollut. Control Assoc.* **1975**, *25* (11), 1145–1147.
(12) Baldauf, R. W.; Heist, D.; Isakov, V.; Perry, S.; Hagler, G. S. W.; Kimbrough, S.; Shores, R.; Black, K.; Brixey, L. *Atmos. Environ.* **2013**, *64*, 169–178.
(13) Venkatram, A.; Snyder, M.; Isakov, V.; Kimbrough, S. *Atmos. Environ.* **2013**, *80*, 248–258.
(14) Venkatram, A.; Horst, T. W. *Atmos. Environ.* **2006**, *40* (13), 2401–2408.
(15) United States Environmental Protection Agency (USEPA). *Rep. No. EPA-454/B-95-003b* **1995**, *2* (September), 1–128.
(16) Heist, D. K.; Perry, S. G.; Brixey, L. a. *Atmos. Environ.* **2009**, *43* (32), 5101–5111.
(17) Venkatram, A.; Snyder, M. G.; Heist, D. K.; Perry, S. G.; Petersen, W. B.; Isakov, V. *Atmos. Environ.* **2013**, *77*, 846–855.
(18) Venkatram, A. *Atmos. Environ.* **2008**, *42* (28), 6862–6868.